submitted to *Geophys. J. Int.*

Supplementary information for the paper "Confirmation of a change in the global shear velocity pattern at 1,000 km depth"

S. Durand[1,2], E. Debayle[1], Y. Ricard[1], C. Zaroli[3] and S. Lambotte[3]

[1] *Laboratoire de Géologie de Lyon - Terre, Planètes, Environnement,*

CNRS, UMR 5276, École Normale Supérieure de Lyon, Université de Lyon,

Université Claude Bernard Lyon 1, 2 rue Raphaël Dubois, Bâtiment Géode 69622 Villeurbanne Cedex, France

[2] *Institut für Geophysik, Corrensstr. 24, 48149 Münster, Deutschland*

[3] *Institut de Physique du Globe de Strasbourg, UMR 7516, Université de Strasbourg, EOST/CNRS, Strasbourg, France*

REFERENCES

French, S.W., Romanowicz, B., 2014, Whole-mantle radially anisotropic shear-velocity structure from spectral-element waveform tomography, *Geophys. J Int.*, , **199**, 1303-1327.

Moulik, P., Ekstrm, G., 2014, An anisotropic shear velocity model of the Earth's mantle using normal modes, body waves, surface waves and long-period waveforms, *Geophys. J Int.*, , **199**3, 1713-1738.

Ritsema, J., Deuss, A., van Heijst, H.J., Woodhouse, J.H., 2011, S40RTS: a degree-40 shear-velocity model for the mantle from new Rayleigh wave dispersion, teleseismic traveltime and normal-mode splitting function measurements, *Geophys. J Int.*, , **184**, 1223-1236.

This paper has been produced using the Blackwell Scientific Publications GJI LaTeX2e class file.

Table 1. Dataset of self-coupling normal mode used in the inversion (inner core sensitive modes have been excluded).

Branch	Modes
0	${}_{0}S_{6}$...${}_{0}S_{60}$
1	${}_{1}S_{2}$...${}_{1}S_{10}$, ${}_{1}S_{11}$...${}_{1}S_{16}$
2	${}_{2}S_{4}$...${}_{2}S_{16}$, ${}_{2}S_{25}$
3	${}_{3}S_{6}$...${}_{3}S_{9}$, ${}_{3}S_{25}$...${}_{3}S_{26}$
4	${}_{4}S_{2}$...${}_{4}S_{5}$
5	${}_{5}S_{3}$...${}_{5}S_{8}$, ${}_{5}S_{11}$-${}_{5}S_{12}$, ${}_{5}S_{14}$...${}_{5}S_{17}$
6	${}_{6}S_{9}$...${}_{6}S_{10}$, ${}_{6}S_{15}$, ${}_{6}S_{18}$
7	${}_{7}S_{5}$...${}_{7}S_{9}$
8	${}_{8}S_{6}$...${}_{8}S_{7}$, ${}_{8}S_{10}$
9	${}_{9}S_{8}$, ${}_{9}S_{10}$...${}_{9}S_{15}$
10	${}_{10}S_{10}$, ${}_{10}S_{17}$...${}_{10}S_{21}$
11	${}_{11}S_{9}$...${}_{11}S_{10}$, ${}_{11}S_{12}$, ${}_{11}S_{14}$, ${}_{11}S_{23}$...${}_{11}S_{25}$
12	${}_{12}S_{6}$...${}_{12}S_{7}$, ${}_{12}S_{11}$...${}_{12}S_{17}$
13	${}_{13}S_{15}$...${}_{13}S_{16}$, ${}_{13}S_{18}$...${}_{13}S_{20}$
14	${}_{14}S_{8}$...${}_{14}S_{9}$, ${}_{14}S_{14}$
15	${}_{15}S_{12}$, ${}_{15}S_{15}$...${}_{15}S_{16}$
16	${}_{16}S_{10}$...${}_{16}S_{11}$, ${}_{16}S_{14}$
17	${}_{17}S_{12}$...${}_{17}S_{15}$
18	-
19	${}_{19}S_{10}$...${}_{19}S_{11}$

Table 2. Dataset of Cross-coupling normal mode used in the inversion (inner core sensitive modes have been excluded).

Branch	Modes
0	${}_{0}S_{11}$-${}_{2}S_{7}$, ${}_{0}S_{14}$-${}_{2}S_{9}$, ${}_{0}S_{17}$-${}_{2}S_{11}$
1	${}_{1}S_{3}$-${}_{3}S_{1}$
2	${}_{2}S_{8}$-${}_{4}S_{3}$, ${}_{2}S_{7}$-${}_{5}S_{5}$, ${}_{2}S_{10}$-${}_{4}S_{5}$
3	${}_{3}S_{7}$-${}_{5}S_{5}$, ${}_{3}S_{8}$-${}_{6}S_{3}$
4	-
5	${}_{5}S_{14}$-${}_{9}S_{8}$, ${}_{5}S_{16}$-${}_{8}S_{10}$
6	${}_{6}S_{15}$-${}_{9}S_{10}$
7	${}_{7}S_{8}$-${}_{5}S_{11}$, ${}_{7}S_{6}$-${}_{6}S_{9}$
8	-
9	${}_{9}S_{6}$-${}_{7}S_{9}$, ${}_{9}S_{12}$-${}_{10}S_{10}$, ${}_{9}S_{14}$-${}_{14}S_{7}$, ${}_{9}S_{15}$-${}_{14}S_{8}$
10	${}_{10}S_{17}$-${}_{11}S_{14}$, ${}_{10}S_{21}$-${}_{12}S_{16}$
11	${}_{11}S_{12}$-${}_{12}S_{11}$, ${}_{11}S_{23}$-${}_{13}S_{18}$
12	${}_{12}S_{12}$-${}_{16}S_{7}$
13	-
14	${}_{14}S_{13}$-${}_{16}S_{11}$
15	${}_{15}S_{16}$-${}_{17}S_{15}$
16	-
17	${}_{17}S_{12}$-${}_{21}S_{7}$

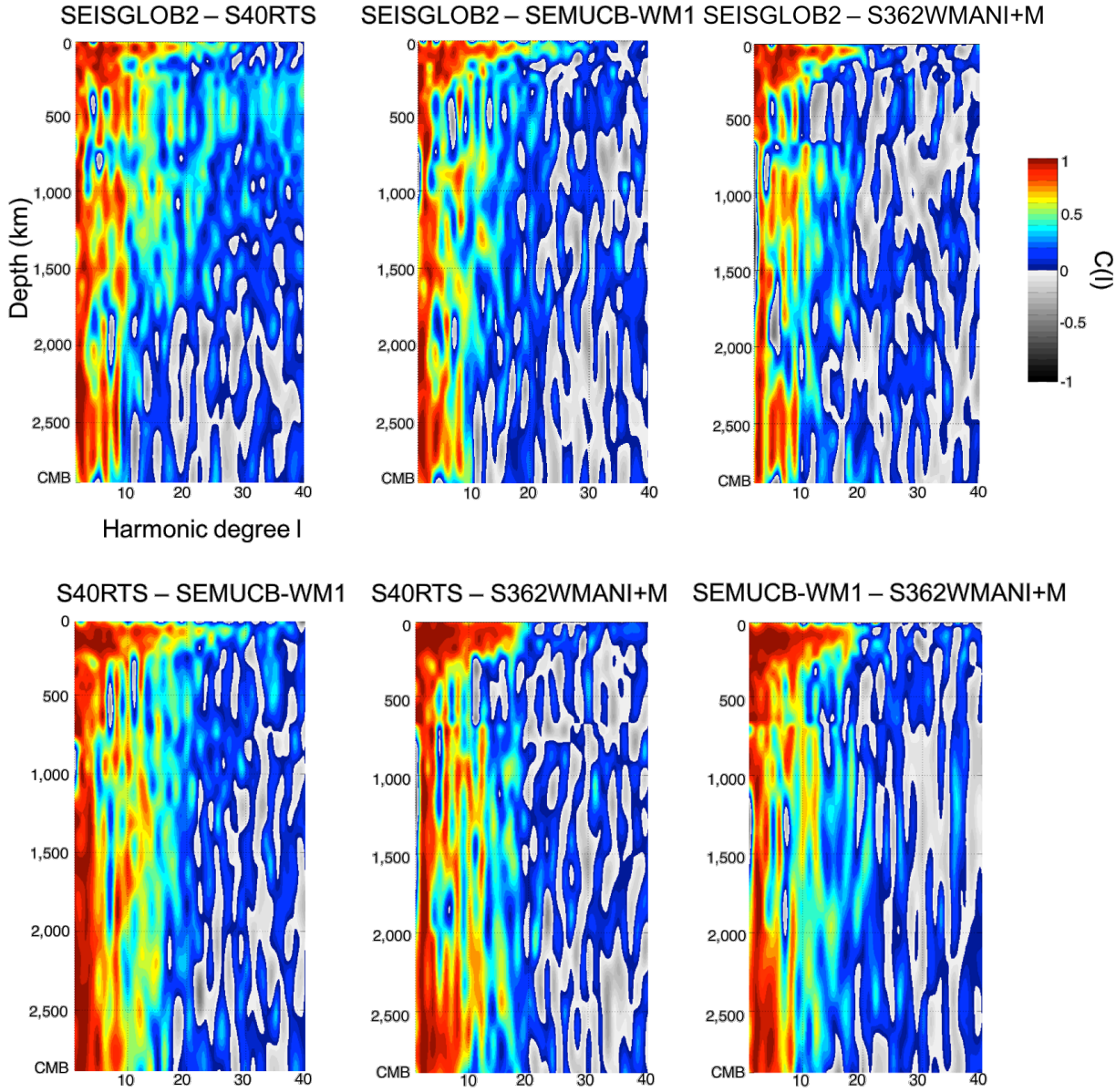

Figure 1. Correlations at various depths between SEISGLOB2 and three recent tomographic models: S40RTS (Ritsema et al., 2011), SEMUCB-WM1 (French & Romanowicz, 2014) and S362WMANI+M (Moulik & Ekström, 2014). For some degrees and depths, the correlations between models can be slightly negative (in gray colors).

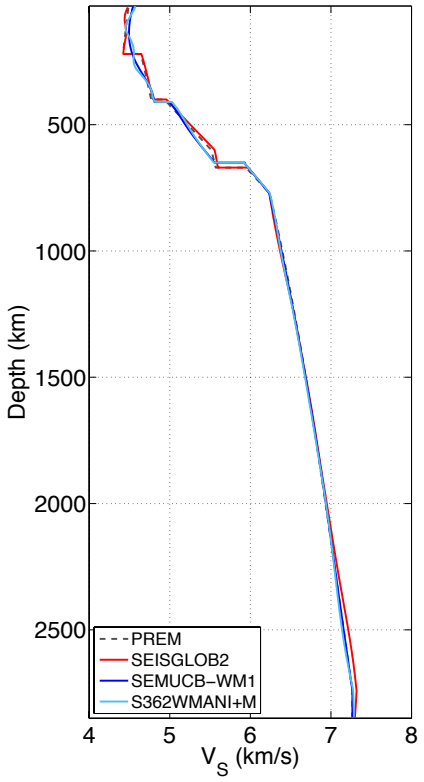

Figure 2. Final shear velocity 1-D models in SEISGLOB2, SEMUCB-WM1 (French & Romanowicz, 2014) and S362WMANI+M (Moulik & Ekström, 2014) compared to PREM. The main differences are located in the upper mantle near 220 km. SEISGLOB2 uses PREM as a 1D initial model and therefore includes the 220 km discontinuity in the final model while SEMUCB-WM1 and S362WMANI+M do not.

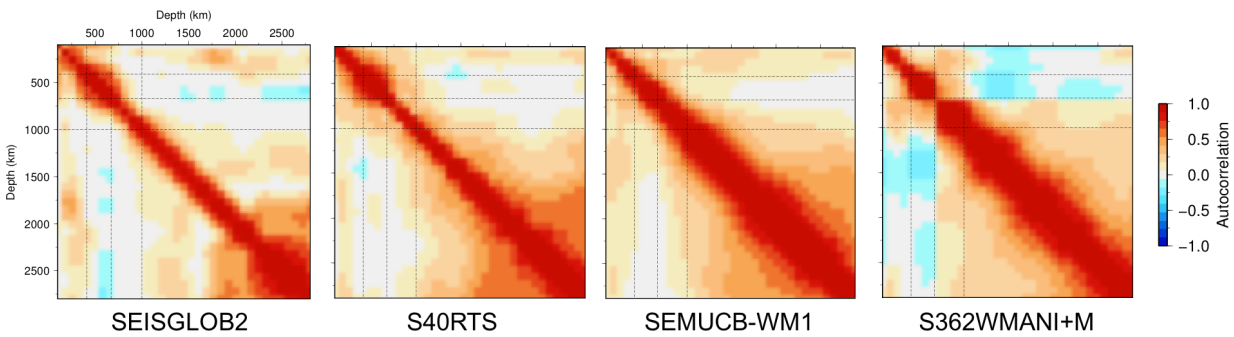

Figure 3. Autocorrelation computed in SEISGLOB2 (left panel) and in three recent tomographic models. The autocorrelation is computed for a depth interval that is equal to the minimum correlation length imposed by the spline basis, namely 80 km. The 410, 670 and 1,000 km depths are indicated by the black dashed lines.